공학석사학위논문

생성 신호를 활용한 해석 가능 인공지능 기반 베어링 고장 주파수 추정에 관한 연구

Study of Interpretable AI Based Bearing Fault Frequency Band Estimation Utilizing Generated Signal

2021 년 02 월

서울대학교 대학원

기계항공공학부

최 종 현

생성 신호를 활용한 해석 가능 인공지능 기반 베어링 고장 주파수 추정에 관한 연구

Study of Interpretable AI Based Bearing Fault Frequency Band Estimation Utilizing Generated Signal

지도교수 윤 병 동

이 논문을 공학석사 학위논문으로 제출함

2020 년 10 월

서울대학교 대학원

기계공학부

최 종 현

최 종 현의 공학석사 학위논문을 인준함

2020 년 12 월

위 원 장 : 김 윤 영 (인)

부위원장 : 윤 병 동 (인)

위 원 : 신 용 대 (인)

공학석사학위논문

생성 신호를 활용한 해석 가능 인공지능 기반 베어링 고장 주파수 추정에 관한 연구

Study of Interpretable AI Based Bearing Fault Frequency Band Estimation Utilizing Generated Signal

2021 년 02 월

서울대학교 대학원

기계항공공학부

최 종 현

Abstract

Study of Interpretable AI Based Bearing Fault Frequency Band Estimation Utilizing Generated Signal

Jonghyun Choi
Department of Mechanical and Aerospace Engineering
The Graduate School
Seoul National University

Selecting a resonance band for demodulation is the most important step in envelope based rolling element bearing diagnosis as the fault impulses modulate to a certain resonant frequency band. To date, many researchers have developed various indicators in multi-domain and use either a binary tree or optimization tool to find the most suitable filter bank with maximum indicator. However, conventional indicator-based methods require specific domain knowledge for choosing the indicator and high computation for calculation since they are based on complex signal processing. To address this issue, this paper suggests a deep learning-based approach using one-dimensional attention gated convolutional neural network(1D-AttGCNN) trained only with a generated signal. The model learns to regress pre-defined resonant parameters of the generated signals and require no additional training when diagnosing a real fault signal. The proposed architecture includes an attention-gated layer, which automatically learns to localize resonance-induced impulse through backpropagation. Moreover, uncertainty and non-Gaussian noise were taken into account in the signal generating process to facilitate the model adaptation to the real target signal. The validity of the proposed model is examined

in various environments with different difficulties via three case studies. Furthermore, comparisons with the conventional Fast Kurtogram and Autogram methods are presented with quantitative measures based on mean absolute deviation distance. Results demonstrate the superiority of the proposed method over the conventional method and the effectiveness of the proposed architecture and signal generation methods.

Keywords: Bearing fault diagnosis
Envelope analysis
Resonance band selection
Attention mechanism
Signal generation
Convolutional neural network

Student Number: 2019-28698

Table of Contents

List of Tables

List of Figures

Chapter 1. Introduction

1.1 Motivation

When a localized fault occurs on a bearing, rolling elements pass through the fault location periodically with a frequency related to the bearing geometry.[1] The extraction of this repetition is one of the most direct health monitoring technique of REB as the component not only inform the overall condition of the bearing but also diagnose the exact defective elements.[2] The repetitive signals are actually the localized impulse produced by contact between rolling elements and faulty areas. The impulse signals are then transmitted to the accelerometer through a specific path in the corresponding system, exciting the structural resonance.[3] However, in a complex mechanical system, the faulty signal is usually submerged in the background noise or signals from other components. Thus, to isolate the signals from noisy components and maximize the bearing fault's periodic information, constructing a bandpass filter with a decent resonant band as a filter bank is crucial. [4] Despite the importance, finding the ground truth of a system's structural resonance is much demanding and almost impossible. Until now, many types of research have been developing signal processing-based indicators and chosen the fault informative band to maximize the indicator.

As a benchmark study, Antoni proposed a spectral kurtosis (SK) based kurtogram method [2]. In the study, SK was used to quantify a certain frequency band's

impulsiveness, as the fault signal of the bearing is commonly presented as localized energy disturbances. Since calculating SK for the full band spectrum is very time-consuming [2] [3], J. Antoni also introduced the Fast Kurtogram (FK) method, which divides filter banks according to a binary tree, rather than calculating SK of all spectrum, and successfully reduced computational cost. [4] Afterward, Tomasz.B proposed Protrugram, which uses the kurtosis of envelope spectrums to measure the energy concentration in a frequency domain to evaluate the periodicity of a certain frequency band.[5] A. Moshrefzadeh proposed Autogram, which uses the SK of the auto-correlation function to consider both periodicity and impulsiveness [6]. Further, in Infogram [7], J. Antoni used negentropy to quantify the fault information of specific frequency band in both time and frequency domain. More recently, A. Mauricio introduced IESFOgram[8] which utilize cyclic Spectral Correlation and Cyclic Spectral Coherence to specify information-rich frequency band under varying operating condition. Although the above-mentioned binary tree-based method has the advantage of real-time band estimation by calculating a certain indicator in discretely separated filter bank, they inevitably extract the sub-optimal result. Thus, many recent studies employed optimization tools to generate optimal band selection results. Zhang and Randall[9] combined a genetic algorithm and FK where the FK presents a rough initial value for the genetic algorithm. Kang et al.[10] also presented a binary-coded genetic algorithm for constructing the optimal bandpass filter, and V. Kannan et al. utilized a real-coded genetic algorithm in [11]. Besides the genetic algorithm, the particle swarm optimization was also suggested as a band selection

tool in [12] and [13] to optimize fault to signal ratio and extract the most informative frequency band.

From the above literature reviews, many researchers have proposed a number of indicators in both the frequency domain and the time domain to select the optimal resonance frequency band. Since these indicators measure the indirect characteristics of the faulty resonant band[14], e.g., periodicity or impulsiveness, the characteristics of extracted frequency band will vary depending on the indicator when diagnosing the bearing fault in an actual engineering field; accordingly, the diagnosis results will be highly dependent on the subjective indicator decision. Furthermore, as the proposed indicators demanded a large amount of computation, such as a time-frequency representation, the trade-off between optimality and real-time estimation were unable to be solved simultaneously by the previous indicator-based method.

To address the issues, this thesis suggested an explainable artificial intelligence-based band selection method utilizing the generated signal.

1.2 Research Scope and Overview

This paper suggests the one-dimensional attention gated convolutional neural networks(1D-AttGCNN) based method trained only with generated signals to select the fault-related resonance band. The 1D-AttGCNN model is suggested to estimate the resonant parameters from a high dimensional raw signal without any preprocessing process or feature engineering, which enables indicator-free band

estimation. Furthermore, the proposed 1D-AttGCNN includes the attention gated layer inspired by [15] to localize the bearing-related impulse effectively in the training process and result interpretation in the inference step.

Though the 1D-AttGCN can directly bridge the resonant band and input signal, labeling with the actual resonant frequency band and acquiring multiple signals with different resonant bands over a wide range of frequency are impossible in real conditions. Thus, this study utilized the generated signal as an input and facilitated pre-definition of the strict resonance region over a wide range of the spectrum. The utilized signal generation process includes non-gaussian noise implementation to imitate the arbitrariness of the real environment. Furthermore, since the proposed method directly estimates the resonance of the real signal without adapting process, real-time and optimal selection are possible.

1.3 Thesis Layout

This paper is structured as follows: In section II, background knowledge regarding deep learning techniques used in this study will be suggested, including a detailed explanation of one-dimensional convolutional neural networks and an attention gated layer. In section III, a detailed description of the suggested methodology is presented. In section IV, resonant band selection results and corresponding diagnosis results for three case studies are presented. In section VI, discussions regarding the attention gated layers and signal generation process are presented.

Finally, contributions and suggestions for futures studies are presented in the conclusion section.

Chapter 2. Background knowledge

This chapter presents background knowledge for this thesis: (1)Envelope analysis, (2) One-dimensional convolutional neural networks, and (3) attention gated layer.

2.1 Envelope analysis

The bearing fault characteristics are often presented as periodic impulse modulated to certain resonance frequency band as in Figure 1.

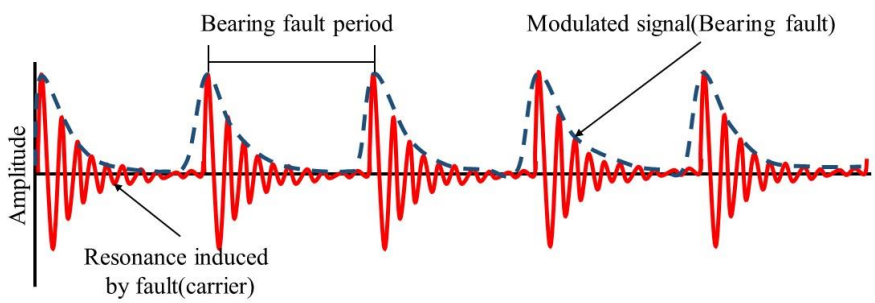

Figure 1 Characteristics of conventional bearing fault signal

As illustrated in Figure 1, typical bearing fault-induced resonance is presented as a periodic signal carrier with a frequency of bearing characteristic components. The signals are often introduced as repetitive transient, in other words, cyclo-stationary. In order to demodulate the signal and extract the fault characteristic components, envelope analysis is the most widely used technique in diagnosing rotating machinery.[16] The common procedure of the envelope analysis is presented in Figure 2. The process includes bandpass filtering for increasing the signal to noise ratio(SNR), Hilbert transform for envelope extraction, and finally fast Fourier

transform(FFT) for envelope spectrum analysis. Fault can be diagnosed in the resulting envelope spectrum by distinguishing fault characteristic(BCF) components from other irrelevant components in the envelope spectrum[16]. Since the SNR of the selected band determines the BCF component's dominance in the final envelope spectrum, the band selection is the most crucial part of envelope analysis[17]. As reviewed in section I, many studies have developed an envelope based bearing fault diagnosis method by advancing the indicator-based band selection method and exposed many issues. To solve such a problem more directly and quickly, this study proposed a deep learning-based technique of 1D-AttGCNN.

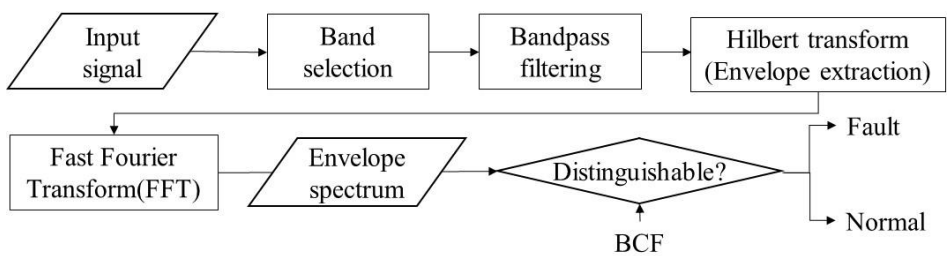

Figure 2 Conventional procedure of envelope analysis

2.2 One dimensional convolutional neural network

Convolutional neural networks(CNN) have been widely used in various industrial fields and showed many promising results in the past decade.[18] CNN has distinct characteristics, which are localized filter operation, weight sharing, and space-wise connection. These aspects allow the CNN to recognize certain patterns from the input while maintaining its spatial information during forwarding propagation.[19] Showing high image processing performance most studies in the bearing diagnostic

field have been adopted CNN as 2-dimensional form.[20]–[23]. However, using 2D-CNN to vibrational signal makes the model more complex and requires an additional 1D to 2D conversion process(e.g., time-frequency representation), which may cause losing some useful information[24]. Therefore, recent studies using vibrational signals, 1D-CNN instead of 2D are often used. Figure 3 demonstrates conventional 1D-CNN architecture.

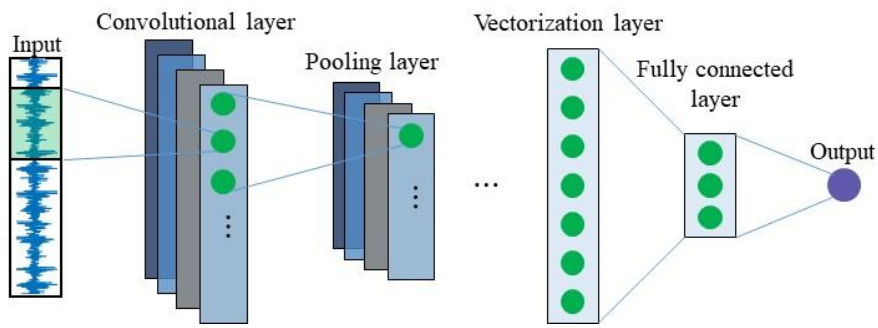

Figure 3 Conventional 1D-CNN architecture

The 1D-CNN architectures are conventionally composed of convolutional layers, pooling layers, vectorization layers, and fully connected(FC) layers. Further mathematical explanation will be presented in the following section

2.2.1 Convolutional layer

The convolutional layers convolve localized filters spatially with input sequence. The input N-dimensional sequence is assumed to be $X = [X_1, X_2, X_3 \dots, X_{\mathrm{N}}]$. The output of a convolutional operation with a l by n filter can be represented as a multiplication between localized input sequence $X_{\mathrm{i:i+l-1}} = [X_i,\ X_{i+1}, \dots, X_{i+l-1}]$

and a kernel $w_j \in R^l$. Final output of the convolutional layer can be denoted as,

$$z_{j,i} = F\left(w_j^T X_{i:i+l-1} + b\right), z \in R^{(N-l+1)\times n}$$

where superscript T corresponds to transpose operation, b and F represent bias, non-linear activation function. A stride is set as 1 for mathematical simplification. By sliding the filter w from $i = 1$ to $N - L + 1$ the final activation map of the j^{th} channel, z_j, can be calculated as,

$$z_j = \left[z_j^1, z_j^2, z_j^3, \dots, z_j^{N-l+1}\right], z \in R^{(N-l+1)\times n}$$

Following the convolutional layer, a pooling layer is applied to extract the most significant local activation map from the output of the convolutional layers while remarkably reducing the dimensionality of the feature space. The j^{th} pooling operation with length g and pooled activation map, p_j^k and P_j, can be obtained as,

$$p_j^k = MAX\left(z_j^{(k-1)g+1}, z_j^{(k-1)g+2}, \dots, z_j^{kg}\right)$$

$$P_j = \left[p_j^1, p_j^2, p_j^3 \dots, p_j^s\right], P \in R^{(N-l+1)\times n}$$

where stride is considered as 1 for a mathematical explanation. Multiple convolutional and pooling layers are constructed for final feature space to consider both low and high-level features from the input sequence.

2.2.2 The global average pooling layer

After a few convolutional layers and pooling layers, the constructed feature maps are vectorized and fed into FC layers for bridging the features with the desired output. The vectorizing process used in this study is global average pooling(GAP), which averages each feature map spatial wisely as,

$$f_j = Avg\left(P_j\right), f \in R^{1\times n}$$

where, Avg corresponds to averaging operation and f_j is j^{th} output of global average pooling layer. By this process, GAP summarizes the information channel

wisely and reduces the dimension of the final feature space before fed into the fully connected(FC) layers. The connected FC layer Consequently, the GAP layer increases regularization and decreases computational cost by contracting the number of parameters.

2.3 The attention mechanism

To assist the baseline CNN model to focus more on the resonance-related impulse rather than irrelevant regions such as noises, an attention mechanism is utilized in this study. The attention mechanism [15] makes a baseline model concentrate on a result-relevant region by applying certain weight to the feature space. In this study, the weight applying layer is denoted as attention gated layer and constructed by combining two convolutional layers without pooling and a locally connected layer. The mathematical explanation of the locally connected layer and attention scoring will be presented in the following section, whereas a detailed architecture will be presented in section 3.2.

2.3.1 The locally connected layer

The locally connected layer is similar to the convolutional layer in the local connection between input and output, except that filters with different weights are applied to each segment. The main difference between a locally connected layer and a convolutional layer is shown in Figure 3.

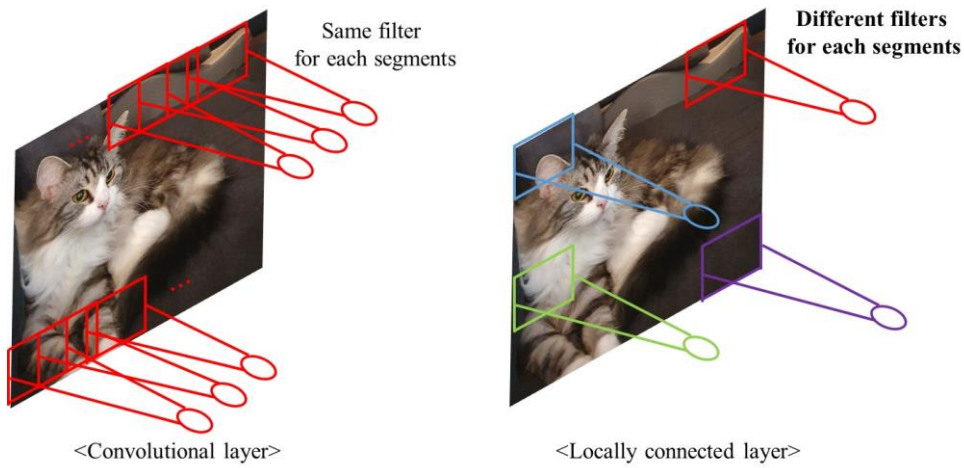

Figure 3 Comparison between convolutional layer and locally connected layer

The mathematical explanation of locally connected layer with filter size l, stride 1, bias b_{LC} and activation function F_{LC} can be denoted as,

$$s_{j,i} = F_{LC}(w_{j,i}^{T} X_{i:i+l-1} + b_{LC})$$

where $w_{j,i}$ and $s_{j,i}$ ith filter and output of j^{th} channel. Unlike convolutional layers the locally connected layer convolve individual filters $w_{j,i}$ for each ith input segment $X_{i:i+l-1}$. Through this process, the locally connected layer exploits different patterns from localized segments while maintaining spatial information. By applying the locally connected layer to the attention-gated layer, the proposed attention gated layer tried to use convolutional layers' overall pattern recognition capability and locally connected layer's local information realization capability complementarily.

2.3.2 The attention scoring

The total attention weighting process by the attention-gated layers is illustrated

in figure 4. The mathematical explanation is as follows.

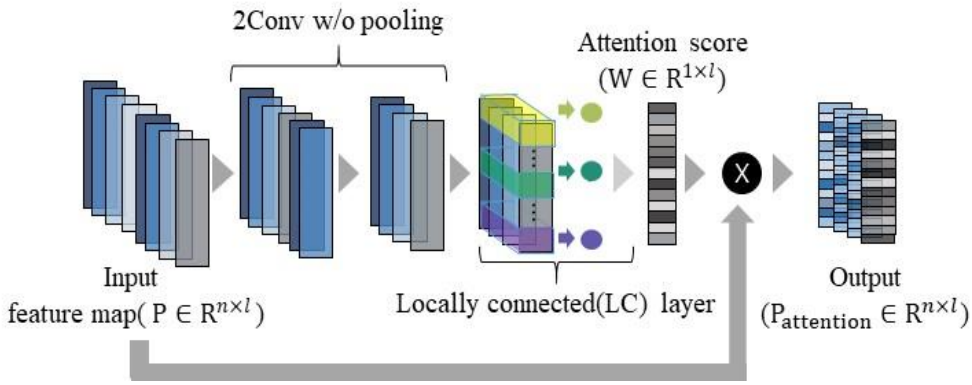

Figure 4 Attention gated layer illustration

Let P the final n by l feature space constructed by the baseline 1D-CNN, then P can be denoted as,

$$P^j = [\mathrm{p}_1^{\mathrm{j}}, \mathrm{p}_2^{\mathrm{j}}, \mathrm{p}_3^{\mathrm{j}}, \dots, \mathrm{p}_{\mathrm{n}}^{j}] \,, \mathrm{P} \in \mathrm{R}^{n \times l}$$

where $\mathrm{p}_i^{\mathrm{j}}$ denotes the i$^{\mathrm{th}}$ feature of j$^{\mathrm{th}}$ channel. The attention score W can be calculated as,

$$W = \mathrm{O}(\mathrm{LC}\left(\mathrm{Conv}\left(\mathrm{Conv}(P)\right)\right))), \mathrm{W} \in \mathrm{R}^{n \times 1}$$

where Conv(P), LC(P) and O(P) stand for the convolutional layers, the one-channel locally connected layer and sigmoid activation function. The sigmoid function is adapted for bounding the attention score 0 to 1. The calculated attention score are multiplied to the input feature space P spatial wisely as,

$$P_{\mathrm{attention}}^{\mathrm{i}} = \mathrm{W} \times [p_1^i, p_2^i, p_3^i, \dots, p_n^i], P_{attention} \in \mathrm{R}^{n \times l}$$

where $P^{i}_{attention}$ denotes the i^{th} attention scored feature space with n-dimensional channels. Through this process, the attention weighted feature map can be constructed by combining the convolutional layers and the attention gated layer. The feature map is then fed into the global average pooling layer and a fully connected layer for output extraction. The attention weighting process can be learned automatically by backpropagation as an ill-posed attention score results in a large gradient flow to the attention gated layer. Furthermore, the score indicates a quantitative concentration of the network in terms of the output. Thus, interpretation of the network's localization result is possible by visualizing the attention score, making the baseline deep learning model more explanatory.

Chapter 3. The proposed 1D-AttGCNN based method

In this section, the proposed 1D-AttGCNN based resonance band selection framework is described in detail. The overall procedures of the proposed method are illustrated in Figure 5.

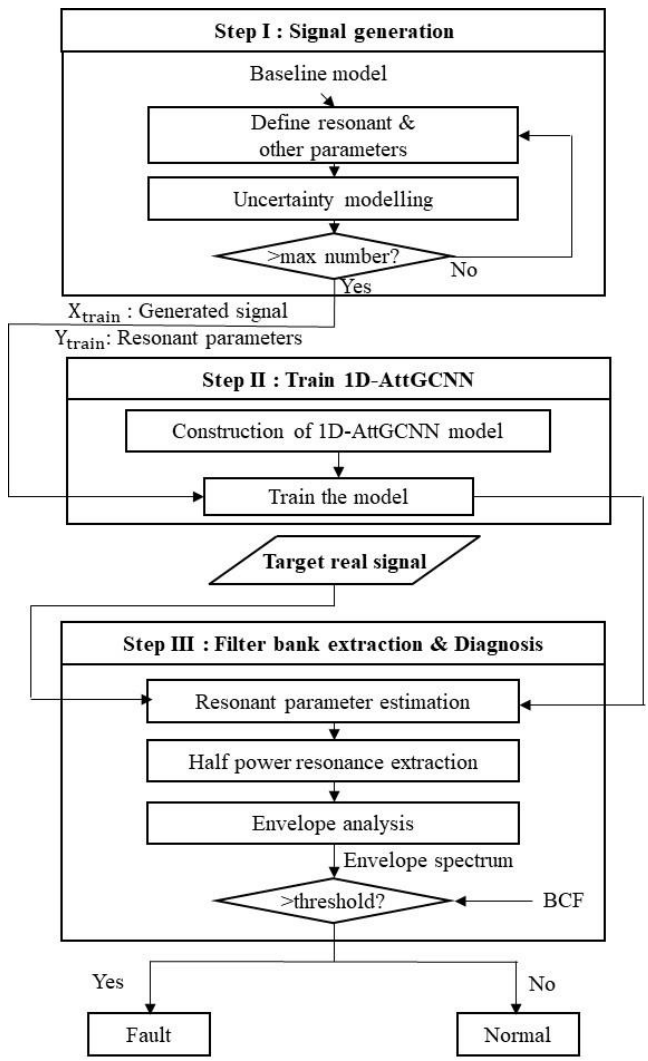

Figure 5 Overall procedure of the proposed method

In step I, signals are generated based on an impulse train model. The uncertainties are taken into account by substituting deterministic parameters as certain random variables with statistically defined distributions. The fake impulses are also implemented arbitrarily to make fault-related impulse localization more challenging. In step II, the 1D-AttCNN model is trained to estimate the resonant parameters of the generated signal. An attention layer is automatically trained to localize the fault impulse. In step III, the resonant parameters of the target input signal are extracted by the trained model and are converted to a bandpass filter bank by half power resonance assumption.[25] Finally, fault is diagnosed by comparing fault frequency component with 6-median absolute deviation(MAD)[26] threshold in the corresponding envelope spectrum.

3.1 Step I: Signal generation

In the signal generation process, the baseline impulse train model can be shown as [1],

$$x(\mathrm{t}) = \Sigma \mathrm{A_i} s\left(t - iT_p\right) + R * \text{white gaussian noise}$$

where,

$$\mathrm{s(t)} = \mathrm{e}^{\beta \mathrm{t}} \sin(2\pi f_n t)\,, A_i = \mathrm{B}\cos(2\pi f_r t) + 1 - B$$

In the above equations, β corresponds to the damping coefficients, $\mathrm{f_n}$ corresponds to the natural frequency, L is signal length, $\mathrm{A_i}$ is the amplitude of $\mathrm{i^{th}}$ impulse R is a Gaussian noise ratio, B is a modulation coefficient which is zero for un-modulated signal, and T is the time interval between fault impulses. Dividing

sampling frequency by T results in the pre-defined fault frequency.

However, the resonant parameters react sensitively to the small changes in a passage that the signal passes through to the sensors. Thus, the resonant parameters should not be treated as a deterministic variable as defined in the baseline signal, but a stochastic variable[27]. Furthermore, the period of fault impulses, T_p, contains uncertainty due to slippage of the rolling element [2] and amplitude of fault impulse, A, contains uncertainty due to curvedness of bearing and sensor voltages.

Thus, to facilitate the adaptation of the trained model to the real signal, these uncertainties are implemented by modeling each parameter of the baseline signal as statistical random variables as equation Table 1.

Table 1 Implemented uncertainties for baseline signal

Parameters	**distribution**	**Source**
$\mathrm{A_i}$	$\mathrm{N}(1,0.1)$	Race way curvedness
T_p	$\mathrm{U}(\mathrm{T_p}, 0.05\mathrm{T_p})$	Slippage of ball
β	$\mathrm{N}(\mu_\beta, \sigma_\beta)$	Resonance passage
f_n	$\mathrm{N}(\mu_n, \sigma_\mathrm{n})$	Resonance passage
f_r	$\mathrm{N}(f_r, 0.05 * f_r)$	Load zone distribution

Whether the designated distribution is suitable for expressing the resonant parameter is not the scope of this study. Instead, the purpose of this uncertainty modeling is to increase the resonance selection capability of the deep learning model by decreasing the gap between the simulation model and the real fault signal in terms

of arbitrariness.

Furthermore, in many previous studies, energy disturbance in time and frequency domain often perturbs band selection result, and these disturbances are often described as non-Gaussian noise.[27]–[29] Thus, to make the regression model robust to presence of energy disturbance in time and frequency domain, the non-Gaussian noise defined as,

$$ngn(\mathrm{t}) = \Sigma \mathrm{K} * \mathrm{rand} * s_f(t - iT_{rand}), \qquad \mathrm{s_f(t)} = \mathrm{e}^{\beta_f \mathrm{t}} \sin\left(2\pi f_f t\right)$$

where f_f and β_f are considered as a random variable with normal distribution as $\beta_f \sim N(\mu_1, \sigma_1^2)$ and $f_f \sim N(\mu_2, \sigma_2^2)$ similar to $x(t)$. To model non-Gaussian noise as a random impulse in random time step amplitude exitation time T_{rand} are modeled as U(0, signal length), which is uniform distribution within the length of the signal. By applying these non-Gaussian noises the signals are augmented with energy disturbance in both the time and the frequency domain. This augmentation enables the model to regress the fault-resonant parameters regardless of both Gaussian and non-Gaussian noises. The effectiveness of non-Gaussian noise will be presented in section 5.3 .

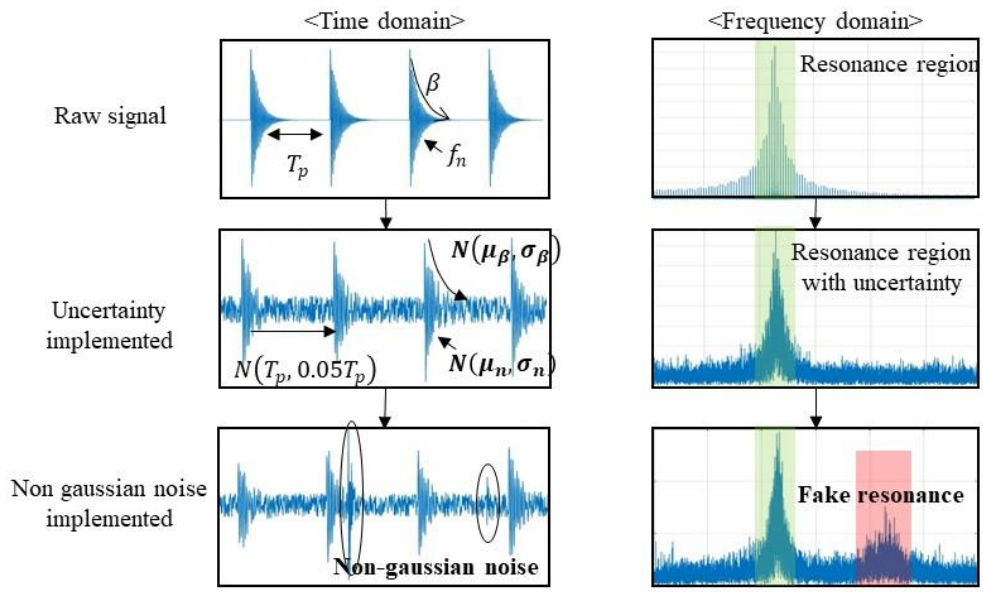

Figure 6 Graphical representation of the signal generation process

Figure 6 graphically demonstrates the effects of the implemented disturbances in both time and frequency domain. The implemented uncertainties apply randomness to both time and frequency domain regarding fault induced resonance. Furthermore, non-gaussian noise, act as arbitrary impulse with normally distributed resonant parameters, excites certain band in frequency domain to challenge the resonant estimation.

For training 30k signals with a length of 6k segments are generated, 15k signals with amplitude modulation as the equation for inner race fault, 15k without modulation for outer race fault. For each signal the parameters were randomly and independently chosen between the upper and lower limit, as shown in Table 2., where Fs is a sampling frequency of the target signal.

Table 2 Upper & lower limits for signal generating parameters

Parameter	**Upper limit**	**Lower limit**
Fs/T(Hz)	250	70
R	3	0.3
μ_f	Fs-500	500
σ_f	$0.3 * \mu_f$	$0.1 * \mu_f$
μ_β	800	100
σ_β	$0.3 * \mu_\beta$	$0.1 * \mu_\beta$
μ_1	Fs-500	500
σ_1	$0.5 * \mu_1$	$0.1 * \mu_1$
μ_2	800	100
σ_2	$0.3 * \mu_\beta$	$0.1 * \mu_\beta$
f_r(Hz)	30	10
K	3	0

3.2 Step II: Train 1D-AttGCNN

In this step, the 1D-AttGCNN is trained to regress the pre-defined mean of natural frequency and damping coefficient of the input signal, μ_n and μ_β. Figure 7 illustrates the architecture and detailed description of the proposed model.

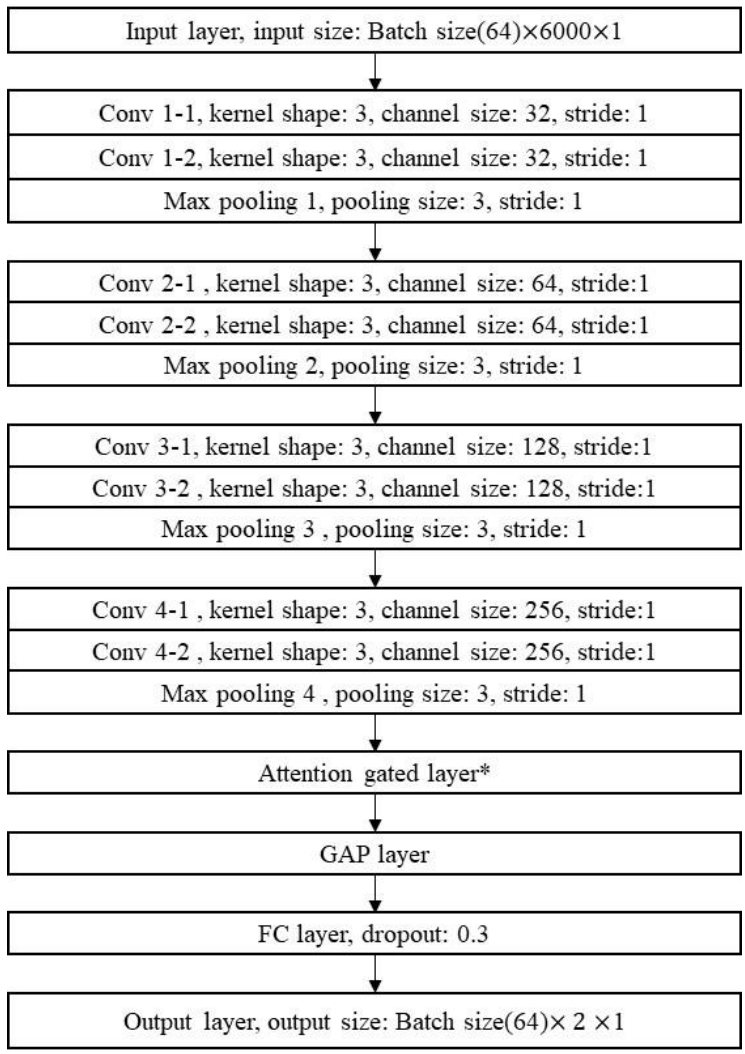

Figure 7 The proposed 1D-AttGCNN architecture

The model is composed of a baseline 1D-VGGNet model and an attention gated layer. The input signal flows through the 1D-VGGNet with ELU activation function and construct feature maps. The feature maps are then propagated to the attention gated layer for attention scoring. After the model constructs an importance-weighted feature map, a global average pooling layer and a fully connected layer with linear activation are used for regression of resonant parameter.

In general, the bearing-related resonance is a localized transient phenomenon within the fault-related impulse; which can be easily masked by irrelevant noise [16]. Thus, applying global time features to estimate resonant parameters may lead to sub-optimal results, due to the irrelevant parts of the signal, such as background noises.[31] Furthermore, the convolutional layers are relatively weak in recognizing localized patterns of the input signal as the layer convolves the same kernels for all input segments. Thus, an attention gated layer is used to highlight the resonance relevant time step and compensate for the baseline VGGNet based CNN in this study.[15]

As presented in section 2.3 proposed attention-gated layer is composed of two 1D-convolutional layers without pooling and one locally connected layer. The detailed illustration of the attention gated layer is as shown in Figure 8.

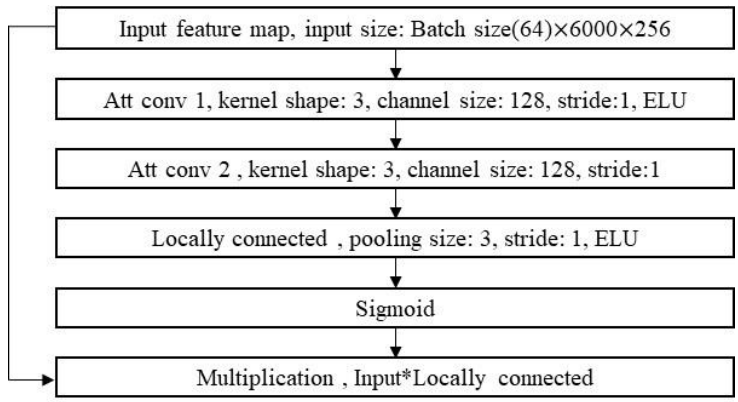

Figure 8 Attention gated layer architecture

By combining convolutional layers and a locally connected layer, the proposed attention gate layer aims to effectively localize the fault-induced resonance, often denoted as periodic transient: The locally connected layer convolves different filters for every input sequence, whereas the convolutional layer uses the same filters. Thus, the locally connected layer is suitable for atoning convolutional layers' vulnerability to local transiencies, such as resonance. In short, this study employs both convolutional layers and locally connected layers simultaneously to recognize localized resonance information within a fault periodic pattern.

As mentioned in section 2.3, the input feature map of the attention gated layers is weighted by the attention score. As the weights correspond to the forward-propagating information scale, the attention layer automatically trains to assign more weight to the resonance-relevance region through backpropagation.

The Figure 7 and 8 also show hyper-parameter settings used for constructing the 1D-AttGCNN. The hyper-parameters of the baseline CNN model are similar to the VGGNet[32]. The stride of every pooling layer is set to 1 so that each segment of the final feature map can point to at least one impulse. The ELU activation function

is used to avoid zero-gradient issues.[33] The channel sizes of the attention gate layer gradually decrease from 64 to 1 to summarize channel-wise information. The detailed training condition and results will be discussed in section 4.

3.3 Step II: Fault diagnosis

In this step, the trained 1D-AttGCNN is used to regress the optimal resonance band of a real signal without further training. This step includes filter bank extraction from the model's output, common procedure of envelope analysis to extract envelope spectrum(ES)[16], and calculation of median absolute deviation(MAD) distance for the quantitative measure.

Even if inputs are from one signal, the estimated results may vary slightly if the 6,000 long segments are from different time steps. Considering the variations, the estimation results from one signal are averaged from the results of fifty randomly divided segments from the signal.

After the parameters are estimated through inference of real signal and averaging, the corresponding band can be calculated using a half-power bandwidth assumption. Then the ratio between the receptance function of arbitrary frequency w and natural frequency w_n is as described in, where δ is a damping ratio.[25]

$$E_r = \frac{\sqrt{(2\delta w_n^2)^2}}{\sqrt{(w_n^2 - w^2)^2 + (2\delta w w_n)^2}}$$

where w_n and δ can be converted by output mean of resonant parameter μ_f and β as,

$$w_n = \sqrt{(2\pi\mu_n)^2 + \mu_\beta^2}\,, \delta = \frac{\mu_\beta}{\sqrt{(2\pi\mu_n)^2 + \mu_\beta^2}}$$

Now assigning w_n and δ into equation E_r, half-power resonant points $f_{resonance}$, which are upper and lower bound of the filter bank can be calculated by solving equation,

$$\frac{2\mu_\beta\sqrt{(2\pi\mu_n)^2+\mu_\beta^2}}{\sqrt{((2\pi\mu_n)^2+\mu_\beta^2-4\pi f_{resonance}{}^2)^2+(4\mu_\beta\pi f_{resonance})^2}}=\frac{1}{2}$$

Once the filter bank is calculated, the common procedure of envelope analysis is used for envelope spectrum extraction, including bandpass filtering, Hilbert-transform, and FFT.

To quantitatively measure the statistical significance of the fault components distinguished in the corresponding envelope spectrum, moving MAD distance is used. The moving MAD is widely used for detecting statistically relevant peak in spectrum analysis,[8] as it is known to be less sensitive to peak outliers than the standard deviation.[26]. The moving MAD value is defined as, [26]

$$\mathrm{MAD(f)} = \mathrm{b} * \mathrm{m}(|\mathrm{X_f} - \mathrm{m}(X_f)|)$$

where b is 1.482, assuming normality of the data,[26] m(x) is the median of signal x, X is the windowed spectrum of the signal divided by 2^7.[26] The MAD distance D for fault frequency component f is defined as equation below.

$$D(f) = \frac{\mathrm{X_f} - m(X_\mathrm{f})}{\mathrm{MAD(X_f)}}$$

The value d measures the statistical distance between extracted fault peak and the median value of i^{th} corresponding window X_i, scaled by MAD. In this study, d value over 6 is set to be diagnostic threshold as 6 similar to 6-sigma rule for detecting outlier.[8]

Chapter 4. Experimental validation

The proposed framework was validated in terms of three case studies. For all three case studies, the proposed networks were trained in computing environment as Table 4.

Table 3 Training environments

Parameters	Condition
GPU	Nvidia Titan XP*2
Loss	Mean squared error
Optimizer	Adam
Learning rate	1e-5
Stop criterion	Minimum validation loss
Max epochs	200
Framework	tensorflow 1.13

The sampling frequencies of the three case studies are different: 10000Hz, 12800Hz, and 48000Hz. Thus, signals with three different Fs values were generated and used individually for AttGCNN training case by case. For comparison, the band selection result and corresponding envelope spectrum of two conventional methods, Fast Kurtogram(FK)[4] and Autogram[6], are also presented for all three cases.

4.1 Case study I: Case western reserve university dataset

In the first case, data sets provided by Case Western Reserve University(CWRU) bearing data center[34] are studied. The bearing test rig of CWRU data center is as Figure 10. Further detail of the test setup can be found in CWRU bearing data center website and reference.[35]

The used CWRU data in this paper are drive end outer and inner race fault data sampled at a frequency of 48,000Hz in, as shown in Table 5. By using 48k dataset, this study aims to verify resonance extraction capability under a wider range of

frequency regions than that of 12k datasets.

Figure 9 Test setup of CWRU dataset

Table 4 Used CWRU data description

Data no	Fault criterion	Fault size (inch)	Speed condition (rpm)	Load condition (HP)	BCF (Hz)
IR007_0	Inner race	0.007	1797rpm	0HP	159.2
OR007@6_0	Outer race	0.007	1797rpm	0HP	107

For the case of outer race fault data, Figure 10 (a) and (b) shows selected frequency band in and corresponding envelope spectrum of the proposed method. The proposed method selected 3721Hz to 3925Hz and distinguished a 107Hz Ball pass frequency outer(BPFO) component well over the 6-MAD threshold. Thus, Figure 10 implies that the proposed method extracted a suitable frequency band for the outer race fault data. Figure 11 and 12 represent the FK and Autogram result for band estimation and envelope spectrum of the outer race fault data. For both conventional methods, the resulted envelope spectrum provided BPFO components well over the threshold. Though the band selection results are significantly different, all three methods

provided a diagnosable BPFO component. This result implies the outer race fault components of the signal are evenly distributed over a wide range of the full spectrum and can be diagnosed in several frequency band.

Figure 13 shows the extracted resonance band for I1 and the corresponding envelope spectrum with the diagnostic 6- MAD threshold of the proposed method. The estimated average natural frequency is 3821Hz, and the damping coefficient is 354, which were converted to a lower limit frequency of 3721Hz and an upper limit frequency of 3925Hz. As shown in Figure 13, the Ball pass frequency inner(BPFI) peak is well above the MAD threshold.

Figure 14 and 15 shows the band selection result and corresponding envelope spectrum of FK and Autgram for the inner race fault data. Both conventional methods extracted frequency band with BPFI higher than the threshold. However, the envelope spectrum of FK and Autogram result shows harmonics of shaft frequency 27.2 Hz as more dominant frequency components than BPFI result. These results imply the bands from FK and Autogram are not based on the faulty impulse but by the shaft induced vibration. Thus, the selection result of FK and Autogram are most likely affected by shaft rotation, not fault induced vibration. These results signify the superiority of the proposed method in terms of fault-related frequency band selection of inner race fault data.

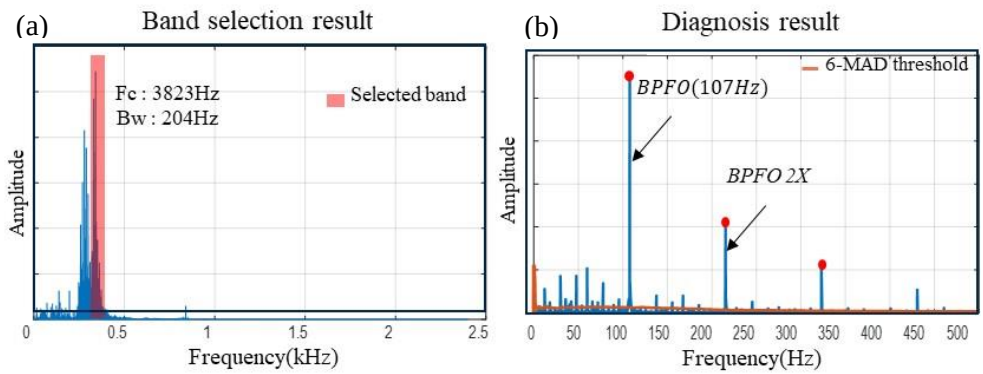

Figure 10 (a) Band selection, (b)diagnosis result of the proposed method for OR data

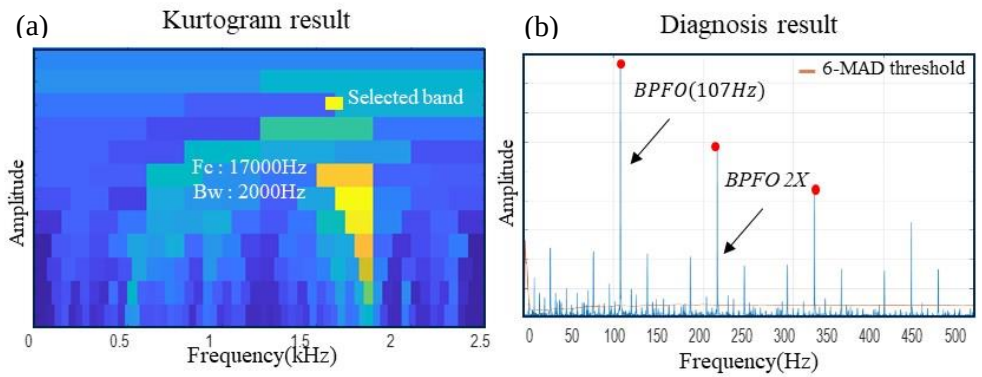

Figure 11 (a) Band selection, (b)diagnosis result of the FK for OR data

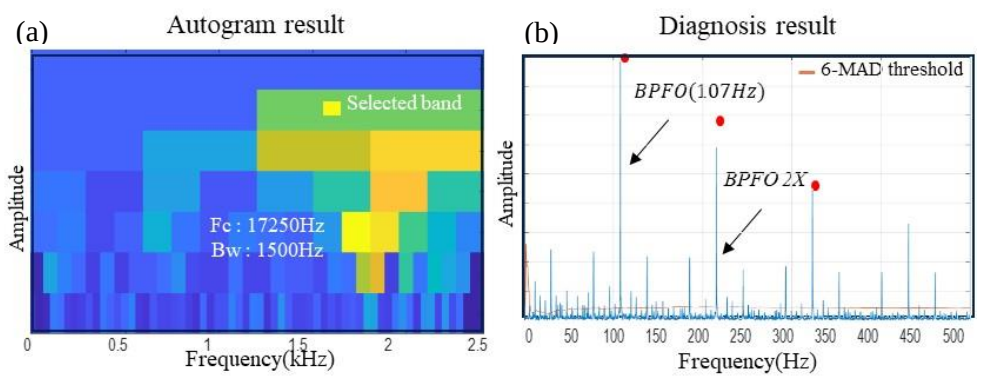

Figure 12 (a) Band selection and (b) diagnosis result of the Autogram for OR data

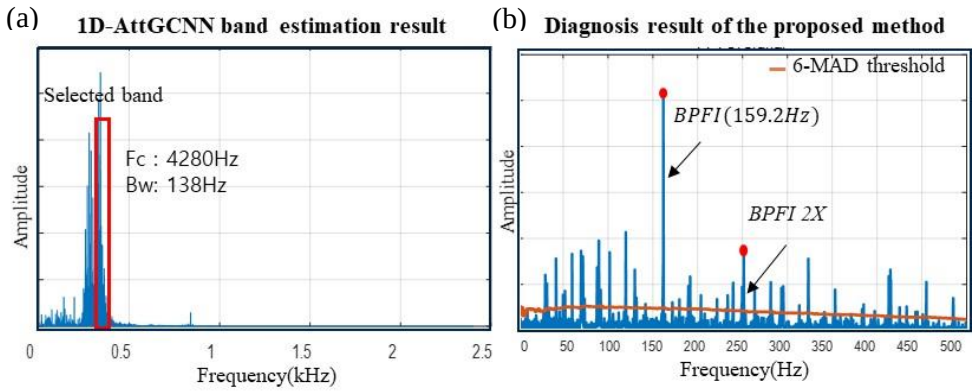

Figure 13(a) Band selection, (b)diagnosis result of the proposed method for IR data

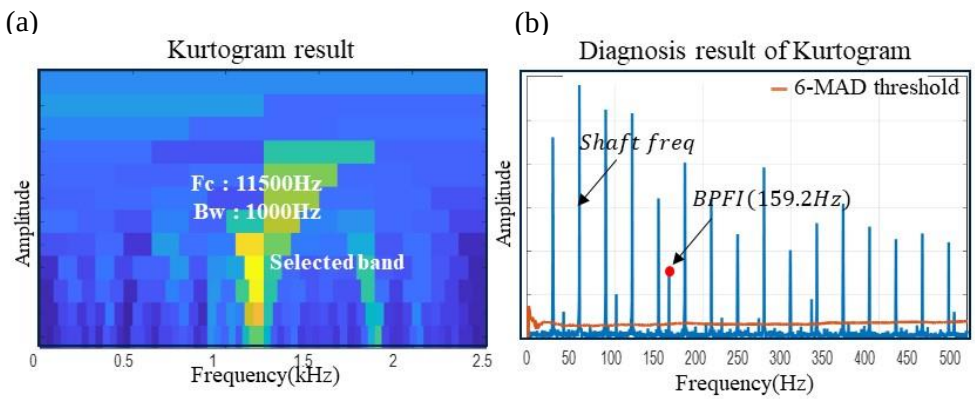

Figure 14 (a) Band selection, (b)diagnosis result of the FK for IR data

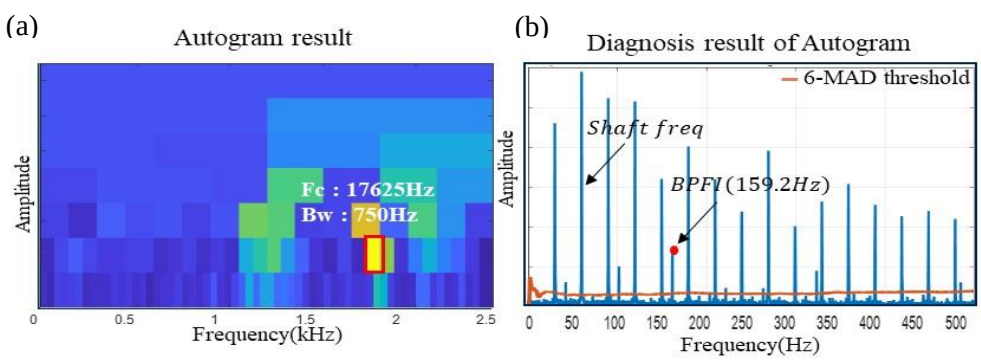

Figure 15 (a) Band selection and (b) diagnosis result of the Autogram for IR data

4.2 Case study II: Seoul national university ALT test

In this case, data acquired from SNU accelerated life test(ALT) test-bed are studied for validation under naturally induced spall and early diagnosis capability. The testbed consists of two support bearings for supporting the shaft, a hydraulic pressure pump for applying loads to radial and axial direction, a motor for rotating the shaft and a 3-axis accelerometer for measuring vibration of the test bearing, as described in Figure 16.

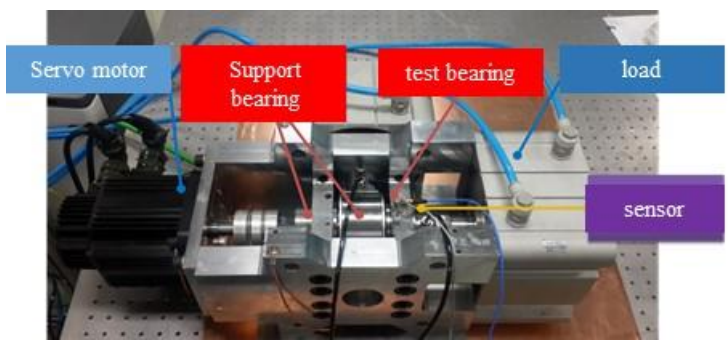

Figure 16 Seoul national university normal to degradation test setup

The accelerometer is mounted vertically on the test bearing housing; thus the resonance condition of the measured signal is highly dependent on the voting condition of the housing. The operating condition and test bearing descriptions are as Table 5[36]. The used data is the acceleration in the vertical direction collected at a sampling frequency of 10000Hz, 10 seconds per minutes. The experiment lasted about 1800 minutes until the RMS value exceeded the empirically set threshold as in Figure 17.

As a result of the experiment, no-fault was induced in the other parts except the inner race. The detailed description of experimental bearing is as Table 5.

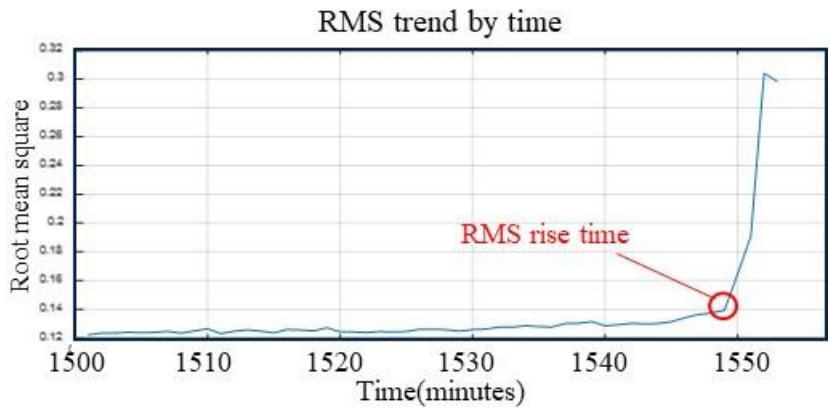

Figure 17 RMS trend of the ALT test

Table 5 Test setup for SNU ALT test

Setup	**Value**
Bearing type	SKF 7202
Speed(RPM)	1450
Axial load(hp)	0.34
Sampling frequency	10000
Expected fault frequency	155.5
Total elapsed time(min)	1552

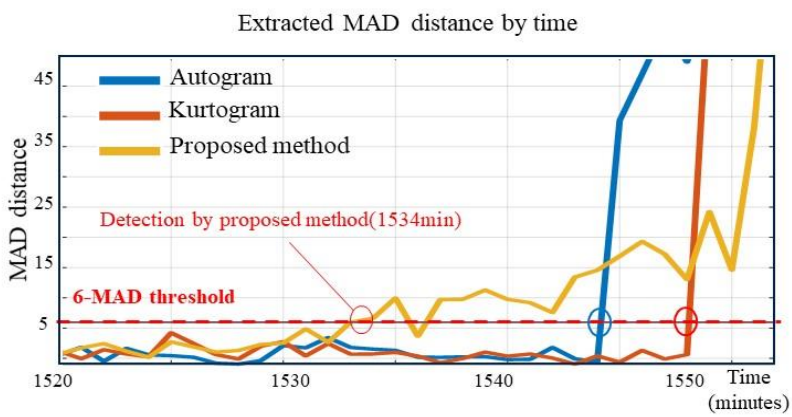

Figure 18 Extracted MAD distance by time(the proposed method, FK, Autogram)

Figure 18 shows the MAD distance threshold of the BPFI extracted from each minute of data of the experiment by the proposed method and two conventional methods. In the figure, the fault frequency components exceeded the MAD threshold at 1534 minutes, 14 minutes before the RMS rise time, whereas FK and Autogram method exceeded at 1546 and 1550 minutes. This result indicates that the proposed two methods cannot estimate the fault informative band early due to their insensitivity, but in the case of the proposed method, a band that maximizes small fault information can be found even at the stage of an incipient small defect.

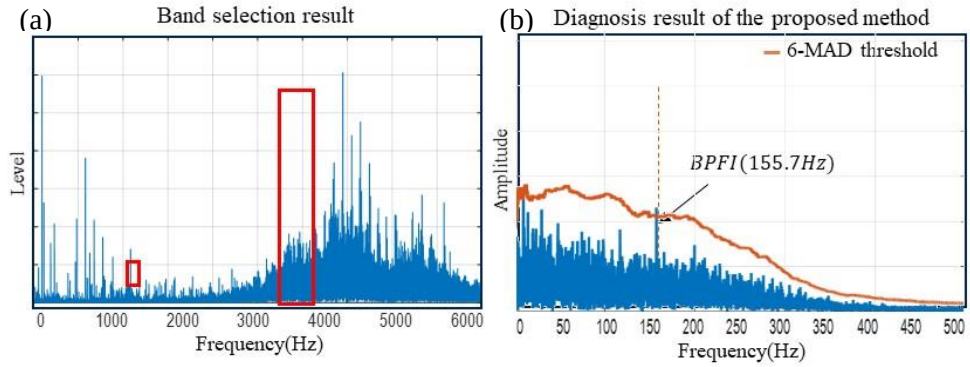

Figure 19 (a)Band selection, (b)diagnosis result of the proposed method for 1534 data

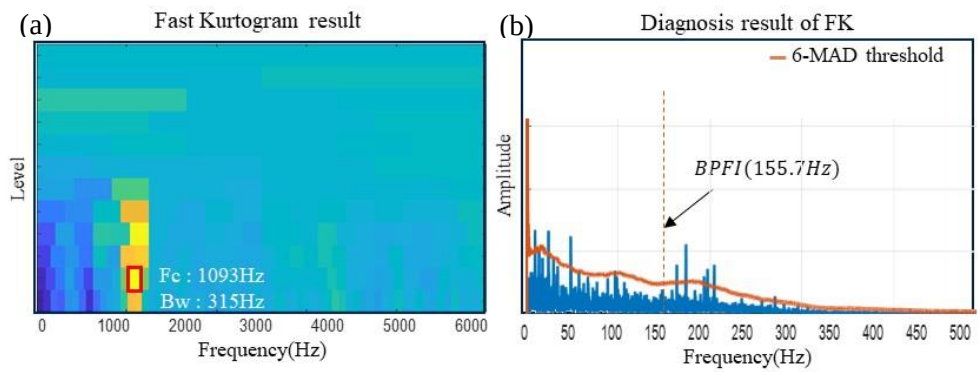

Figure 20 (a) Band selection, (b) diagnosis result of the FK for 1534 data

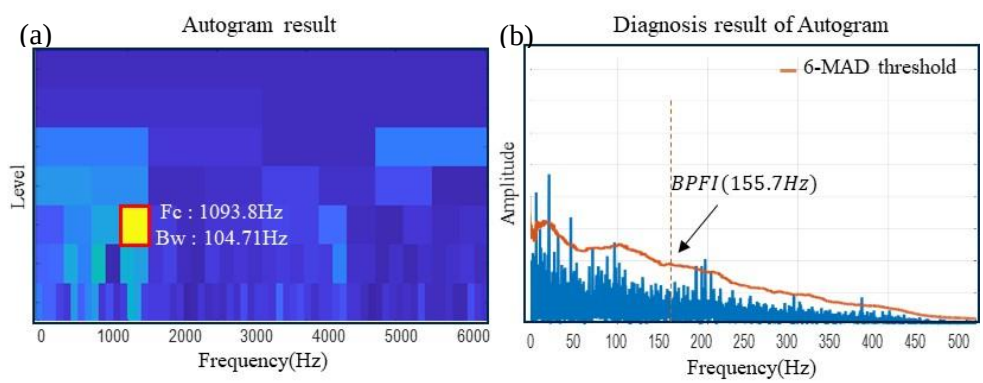

Figure 21 (a) Band selection, (b) diagnosis result of the Autogram for 1534 data

Figure 19 shows the extracted frequency band and corresponding envelope spectrum of the 1534 minutes data, where the proposed method first detects the inner race fault. As in Figure 19 (a), the proposed method selected 3453Hz to 3702Hz as a filter bank, and the BPFI component can well be distinguished from the other components by exceeding the threshold with MAD distance of 7.21313 in the corresponding envelope spectrums. These results clearly show that the proposed method is capable of early diagnosis of initiated incipient fault of inner race.

Based on the Figure 20 and 21, the conventional two method selected un-effective frequency band and failed to diagnose early initiated spall, though the proposed method first extracted the diagnosable BPFI from the same data. From those analysis, the proposed method proved to be more effective in early detection of naturally induced spall than conventional methods.

4.3 Case study III: On-road wheel bearing dataset

The vibration signal from a faulty automobile wheel bearing on real road conditions are analyzed in the last case.

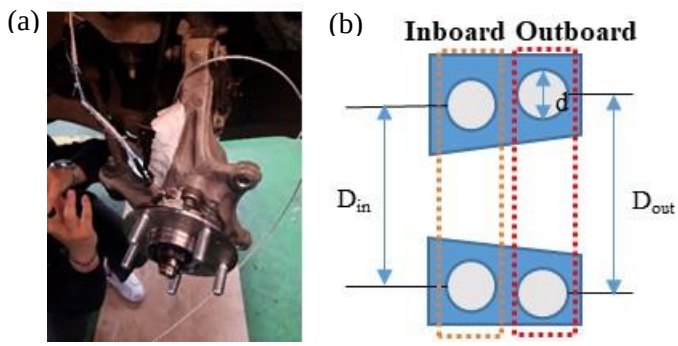

Figure 22 (a) Accelerometer setup, (b) simplified cross-section of wheel bearing

Table 6 Data description

Data no	Environment	Fault location	Vehicle speed	Rotational speed(RPM)	BCF(Hz)
W60	Conventional road	Inboard outer race	60km/h	500	52
W100	Highway	Inboard outer race	100km/h	840	96

Figure 25 shows the simplified cross-section of the target wheel-bearing and table 7 shows the physical properties of the bearing. The fault was seeded by impact hammer to the onboard outer race of the bearing to imitate brinelling. The accelerometer was seeded directly to the target bearing as Figure 25 (a) and measured vibration of 3 directions with a sampling frequency of 12,800Hz. The electric car is used for the experiment to avoid explosive vibration signals from internal combustion engines. The experiment was conducted on two different environments: one on the conventional road with 60km/h constant speed and one on the highway with 100km/h constant speed. The operating conditions and expected fault frequencies can be seen in the table 6. The fault frequencies may show small differences from the theoretical values as the rotation of the shaft has minor fluctuation. Since the data was gathered from bearing mounted on a vehicle operating in a real road environment, strong noises such as structural vibration or road fluctuation are expected to be contained.

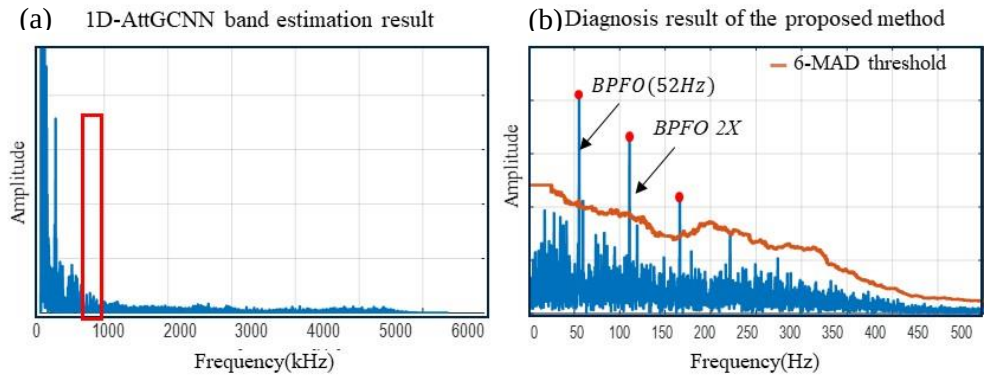

Figure 23 (a)Band selection, (b)diagnosis result of the proposed method for W60 data

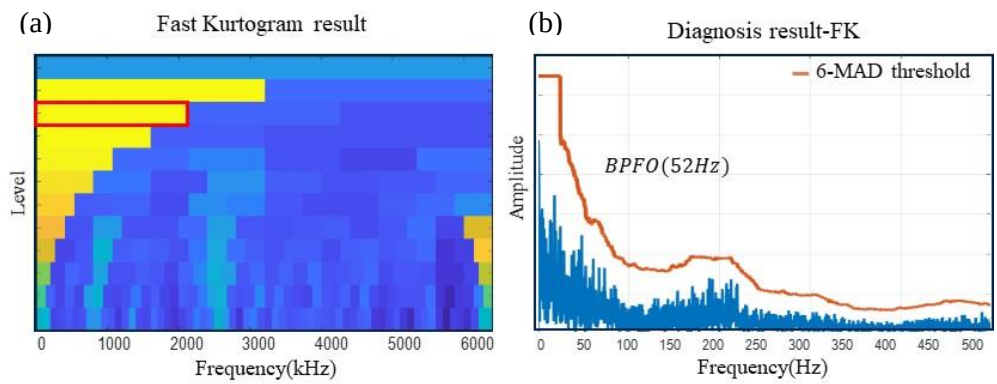

Figure 24(a) Band selection, (b) diagnosis result of FK for W60 data

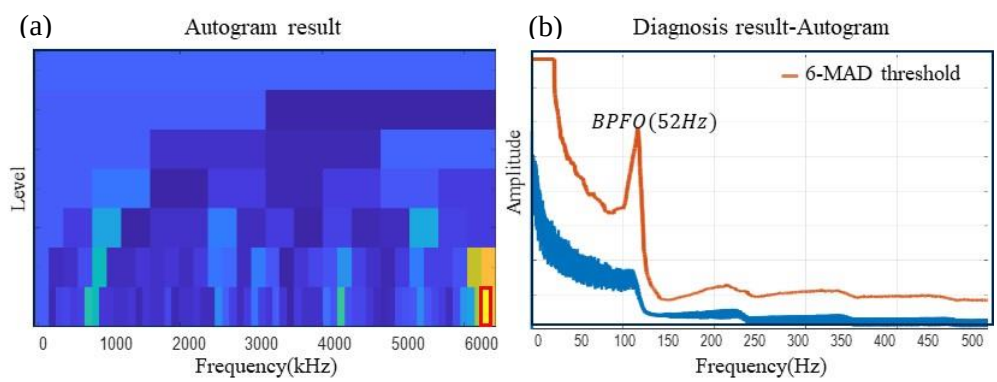

Figure 25 (a) Band selection, (b) diagnosis result of Autogram for W60

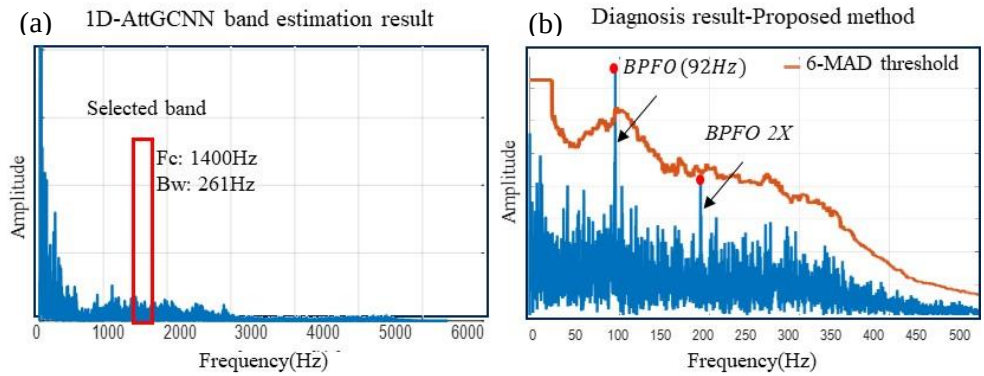

Figure 26 (a)Band selection, (b)diagnosis result of the proposed method for W100 data

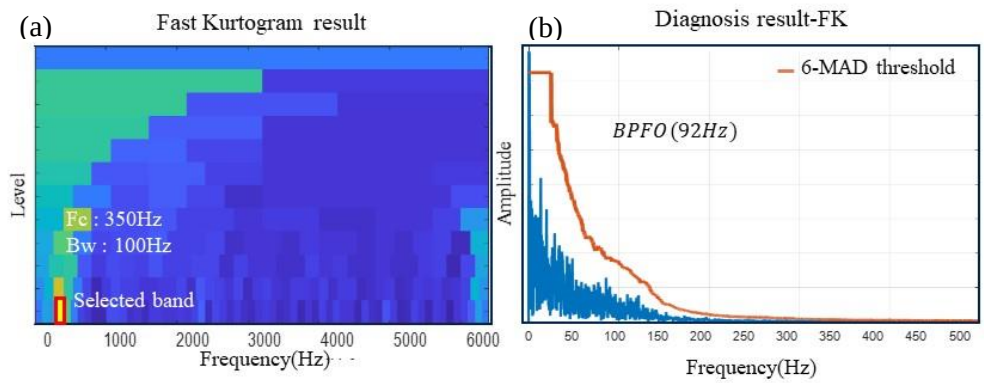

Figure 27 (a) Band selection, (b) diagnosis result of FK for W100 data

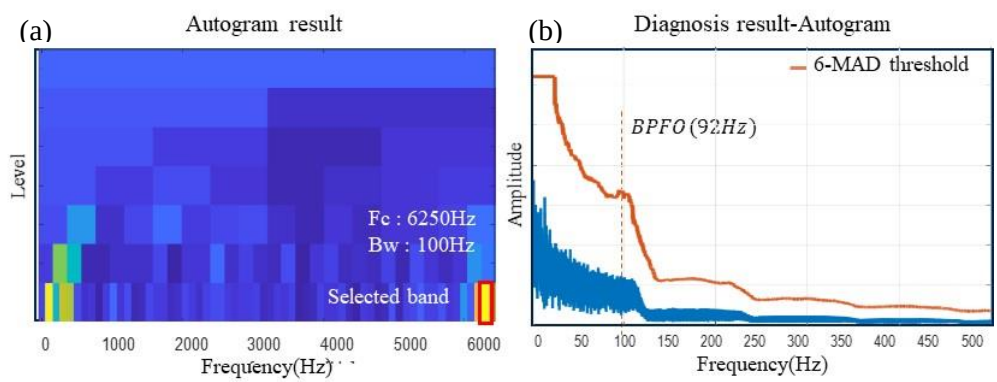

Figure 28(a) Band selection, (b) diagnosis result of Autogram for W100

Figure 23 (a) and (b) represent the band selection and reciprocal envelope spectrum of data W60 result in by the proposed method. Based on the Figure 23, the proposed method selected 811Hz to 1101Hz as filter bank and successfully diagnosed outer race fault with MADD of 12.1. The corresponding envelope spectrum exhibits distinct BPFO and its second harmonic, though the signal contains strong low frequency noise as FFT result Figure 23 (a). Thus, proposed method successfully diagnoses the outer race fault of the onboard bearing on the conventional road.

FK and Autogram result of data W60 and their diagnostic result are described in Figure 24 and 25. As shown in Fig, FK extract high frequency region 6133Hz to 6400Hz as filter bank and demonstrate no distinct fault frequency component over the threshold. Also, as in Figure 25, Autgram selects 3150Hz to 3650Hz region and reveal no fault-related impulse over the threshold.

For W100 dataset, the estimation and its envelope spectrum of the proposed method is as Figure 26. The proposed method selected 1313Hz to 1587Hz for bandpass filtering and exhibit a noticeable BPFO component with 8.771 MADD.

However, as presented in Figure 27 and 28, FK and Autogram chose much lower and higher frequency regions and failed to extract any specific fault-related component, not to mention the threshold. Thus, we can conclude that FK and Autogram choose inadequate frequency bands for outer race fault diagnosis.

Based on the result above, the proposed method shows compatible diagnostic capability under both conventional and highway condition while demonstrating better condition.

Chapter 5. Discussion

In this section, further discussions regarding the case study results will be given. In section 5.1, the effectiveness of the attention gated layer will be discussed in terms of the impulse localization effect by visualizing the attention score and regularization. Also, in section 5.2, the implementation of non-Gaussiafn noise will be further discussed in terms of diagnostic capability under a noisy environment.

5.1 Effectiveness of attention gate layer

For visual interpretation of whether the resonant parameters are chosen based on the fault-related impulse. The attention result will be shown by coloring the raw signal according to the attention scores.

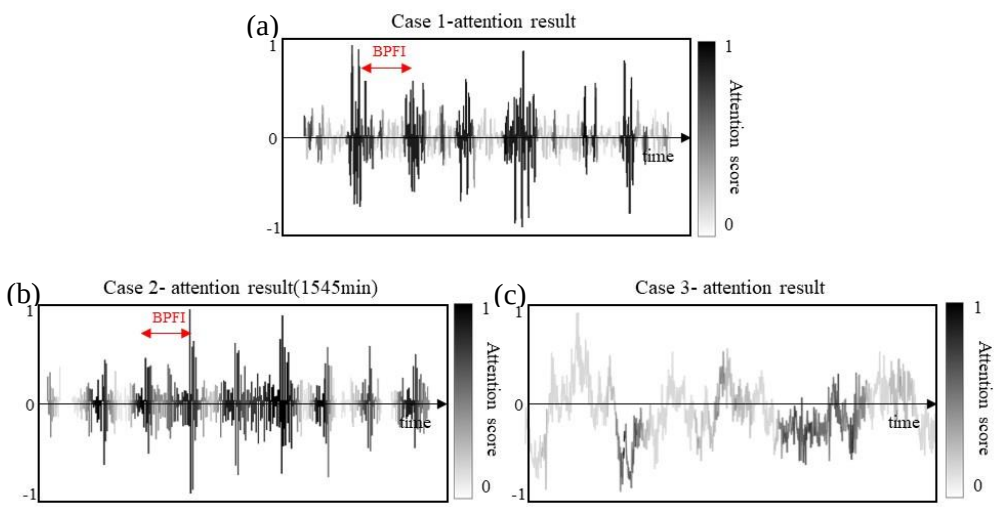

Figure 29 Attention score results of (a) case I: IR data (b) case II: 1552 data and (c) caseIII: W100 data

Figure 29 shows the visualization result of attention scores extracted from case I~III. For cases I and II, the attention-gate layer grant high attention score for the fault related impulse regions, which are spaced with a period related to the BPFI. This clearly shows that the resonant parameters of case I & II are estimated based on the inner race fault induced impulse. However, since the raw signal of case study III is acquired under noisy real environment, the signal retains strong modulation and low frequency noises, which makes visual detection of fault related impulse impossible. Thus, although the attention scores are localized in a certain region, the interpretation of whether the regions are fault-related impulses is relatively difficult . In short, under the experimental condition, the highlighted region of the attention gated layer can be interpreted as the fault-induced impulse, nevertheless it is hard to be certain under noisy environment due to the limitation of visual inspection. Though the visualization result is ambiguous

In figure 30, the training results of the proposed 1D-AttGCNN and 1D-CNN without the attention gated layer are compared.

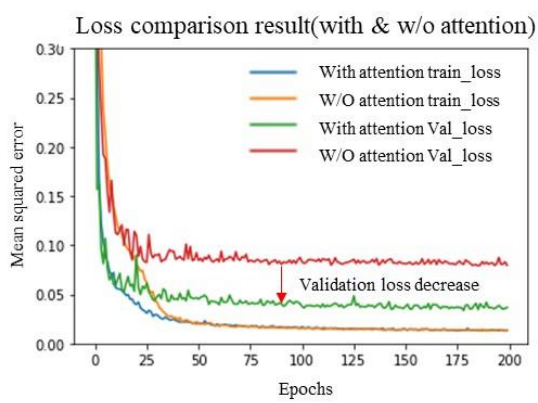

Figure 30 Loss comparison of with and w/o attention gated layer model

Table 7 Band selection comparison between with and w/o attention model

	Case I		Case II		Case III	
	Fc(Hz)	Bw(Hz)	Fc(Hz)	Bw(Hz)	Fc(Hz)	Bw(Hz)
With attention	4280	138	3580	238	1400	261
W/O attention	-98	206	3670	254	-10887	349

The result shows that implementation of the attention-gated layer decrease validation mean squared error(MSE) loss. Also in Table 8, the band estimation result comparison results are given. Without the attention gated layer, the conventional CNN infer negative resonance parameters from case I and III data which are invalid for band passing. These results indicate that the proposed attention-gated layer increases the regularization of the conventional model in both training and test parts.

5.2 Effectiveness of non-Gaussian noise implementation

In this section, the effectiveness of non-gaussian noise implementation will be analyzed in terms of diagnostic capability under a noisy environment. Figure 31 presents a comparison between extracted MAD distance value of 1D-AttGCNN model trained with and without non-gaussian noise implementation.

As Figure 31 shows, the model trained without non-gaussian noises extracted MAD distance lower than the threshold for both W60 and W100 data. This result demonstrates that the non-gaussian implementation increases the model's

compatibility under noisy environment.

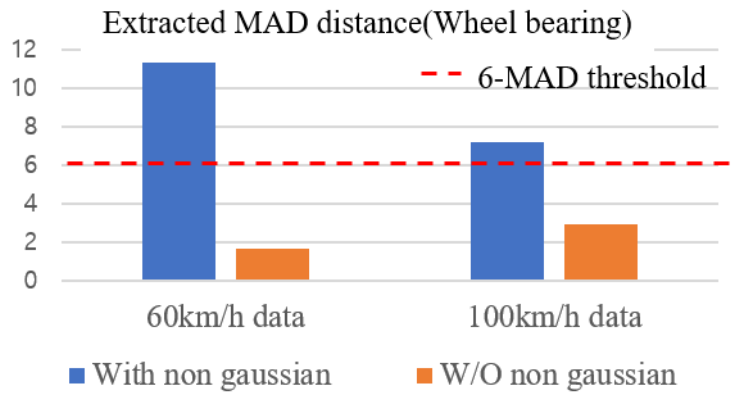

Figure 31 Extracted MAD distance comparison between with and w/o NGN

Chapter 6. Conclusions

6.1 Summary and Contributions

In this thesis, a novel 1D-AttGCNN based bearing fault frequency band estimation method utilizing generated signals in the training step has been proposed. The contributions and significance of this research are summarized as follows.

Contribution 1: Development first direct band selection approach based on deep learning

In this thesis, a 1D-AttGCNN is newly utilized to directly estimates fault resonance frequency band from the raw signal. The band selection is known to be the most important part of the envelope-based fault diagnosis field. However, conventional signal processing based methods have been shown two inevitable issues in terms of indicator dependent result and real-time optimality trade-off. By using a deep neural network, this study constructs direct link between raw bearing signals and their resonant frequency band, which enables objective and real time decision.

Contribution 2: Superior to conventional signal processing based methods in terms of diagnostic capability under various environment

The proposed method has been verified its effectiveness in three different environments by comparing with two conventional methods. The proposed method shows superior diagnostic capability in terms of selecting fault-informative frequency band and extracting distinguishable fault frequency components from

experimental environment to noisy real condition.

Contribution 3: Overcoming black box-ness of conventional deep learning method by attention-gated layer.

The employed attention-gated layer localizes fault-related resonance region by controlling the information through attention score weighting. After the inference, the basis region of the model's estimation can be highlighted by visualizing attention scores. As the CNN preserves localized information during forward passing, highly weighted regions of the final feature maps directly indicate focused regions from the input. These aspects make the baseline CNN model more explanatory.

6.2 Suggestions for Future Research

This thesis proposed a noble 1D-AttGCNN based resonant band selection method. But there still exist several issues to be solved for the advancing deep learning-based band selection. The details of the issues are listed as follows.

Issue 1: Analytic signal generation process

The proposed signal generation steps are composed of simple analytic bearing fault simulation model and several uncertainties. This simplified simulation model enables fast implementation of bearing fault signal. However, in the analytic model. Thus, the proposed signal generation step can be advanced through more complex modeling with physical aspects of bearing defects. For instance, FEM model can imitates not only incipient spalls with different shapes but also sub-surface crack and can generate more adaptable signal to real environment.

Issue 2: Difficulty in visual interpretation under noisy environment

Proposed attention gated layer presented reasonable interpretation in case study 1 & 2. However, for case 3, the interpretation based on visualization was difficult since there exist strong low frequency noises and modulation. This issues are expected to be solved by employing several state of the art XAI(explainable artificial intelligent) techniques. For example, gradients based techniques such as integrated gradients or sensitivity analysis can enhance the interpretation under noisy environments.

Issue 3: Difficulties in parameter setting

The hyper-parameter settings in this study were empirically chosen based on the VGGnet. Though the settings are adequate enough to show the effectiveness of the deep learning based approach, the performance of the proposed 1D-AttGCNN model can further be boosted through hyper-parameter optimization. Recently, Bayesian based approaches such as gaussian process or scalable Bayesian optimization have been utilized for hyper-parameter tuning of the deep neural networks

References

1. P. D. McFadden and J. D. Smith, “Model for the vibration produced by a single point defect in a rolling element bearing,” *J. Sound Vib.*, vol. 96, no. 1, pp. 69–82, 1984.

2. R. B. Randall and J. Antoni, “Rolling element bearing diagnostics-A tutorial,” *Mech. Syst. Signal Process.*, vol. 25, no. 2, pp. 485–520, 2011.

3. J. Antoni and R. B. Randall, “The spectral kurtosis: Application to the vibratory surveillance and diagnostics of rotating machines,” *Mech. Syst. Signal Process.*, vol. 20, no. 2, pp. 308–331, 2006.

4. J. Antoni, “Fast computation of the kurtogram for the detection of transient faults,” *Mech. Syst. Signal Process.*, vol. 21, no. 1, pp. 108–124, 2007.

5. Y. Xu, K. Zhang, C. Ma, L. Cui, and W. Tian, “Adaptive Kurtogram and its applications in rolling bearing fault diagnosis,” *Mech. Syst. Signal Process.*, vol. 130, pp. 87–107, 2019.

6. A. Moshrefzadeh and A. Fasana, “The Autogram: An effective approach for selecting the optimal demodulation band in rolling element bearings diagnosis,” *Mech. Syst. Signal Process.*, vol. 105, pp. 294–318, 2018.

7. J. Antoni, “The infogram: Entropic evidence of the signature of repetitive transients,” *Mech. Syst. Signal Process.*, vol. 74, pp. 73–94, 2016.

8. A. Mauricio, W. A. Smith, R. B. Randall, J. Antoni, and K. Gryllias,

"Improved Envelope Spectrum via Feature Optimisation-gram (IESFOgram): A novel tool for rolling element bearing diagnostics under non-stationary operating conditions," *Mech. Syst. Signal Process.*, vol. 144, p. 106891, 2020.

9. Y. Zhang and R. B. Randall, "Rolling element bearing fault diagnosis based on the combination of genetic algorithms and fast kurtogram," *Mech. Syst. Signal Process.*, vol. 23, no. 5, pp. 1509–1517, 2009.

10. M. Kang, J. Kim, B.-K. Choi, and J.-M. Kim, "Envelope analysis with a genetic algorithm-based adaptive filter bank for bearing fault detection," *J. Acoust. Soc. Am.*, vol. 138, no. 1, pp. EL65–EL70, 2015.

11. V. Kannan, H. Li, and D. V Dao, "Demodulation Band Optimization in Envelope Analysis for Fault Diagnosis of Rolling Element Bearings Using a Real-Coded Genetic Algorithm," *IEEE Access*, vol. 7, p. 1, 2019.

12. K. Yu, T. R. Lin, J. Tan, and H. Ma, "An adaptive sensitive frequency band selection method for empirical wavelet transform and its application in bearing fault diagnosis," *Meas. J. Int. Meas. Confed.*, vol. 134, pp. 375–384, 2019.

13. S. Tyagi and S. K. Panigrahi, "An improved envelope detection method using particle swarm optimisation for rolling element bearing fault diagnosis," *J. Comput. Des. Eng.*, vol. 4, no. 4, pp. 305–317, 2017.

14. T. Barszcz and A. Jabłoński, "A novel method for the optimal band

selection for vibration signal demodulation and comparison with the Kurtogram," *Mech. Syst. Signal Process.*, vol. 25, no. 1, pp. 431–451, 2011.

15. A. Vaswani, N. Shazeer, N. Parmar, J. Uszkoreit, L. Jones, A. N. Gomez, Ł. Kaiser, and I. Polosukhin, "Attention is all you need," *Adv. Neural Inf. Process. Syst.*, vol. 2017-Decem, no. Nips, pp. 5999–6009, 2017.

16. R. B. Randall and J. Antoni, "Rolling element bearing diagnostics-A tutorial," *Mech. Syst. Signal Process.*, vol. 25, no. 2, pp. 485–520, 2011.

17. J. Wodecki, P. Kruczek, A. Bartkowiak, R. Zimroz, and A. Wyłomańska, "Novel method of informative frequency band selection for vibration signal using Nonnegative Matrix Factorization of spectrogram matrix," *Mech. Syst. Signal Process.*, vol. 130, pp. 585–596, 2019.

18. S. Zhang, S. Zhang, B. Wang, and T. G. Habetler, "Deep Learning Algorithms for Bearing Fault Diagnosticsx - A Comprehensive Review," *IEEE Access*, vol. 8, pp. 29857–29881, 2020.

19. H. Wang, J. Xu, R. Yan, C. Sun, and X. Chen, "Intelligent Bearing Fault Diagnosis Using Multi-Head Attention-Based CNN," *Procedia Manuf.*, vol. 49, no. C, pp. 112–118, 2020.

20. L. Wen, X. Li, L. Gao, and Y. Zhang, "A New Convolutional Neural Network Based Data-Driven Fault Diagnosis Method," *IEEE Trans. Ind. Electron.*, vol. 65, no. 7, pp. 1–1, 2017.

21. D. Zhao, T. Wang, and F. Chu, "Deep convolutional neural network based

planet bearing fault classification," *Comput. Ind.*, vol. 107, pp. 59–66, 2019.

22. Z. Chen, A. Mauricio, W. Li, and K. Gryllias, "A deep learning method for bearing fault diagnosis based on Cyclic Spectral Coherence and Convolutional Neural Networks," *Mech. Syst. Signal Process.*, vol. 140, p. 106683, 2020.

23. Z. Xu, C. Li, and Y. Yang, "Fault diagnosis of rolling bearing of wind turbines based on the Variational Mode Decomposition and Deep Convolutional Neural Networks," *Appl. Soft Comput. J.*, vol. 95, p. 106515, 2020.

24. S. Kiranyaz, O. Avci, O. Abdeljaber, T. Ince, M. Gabbouj, and D. J. Inman, "1D convolutional neural networks and applications - A survey," *arXiv*, pp. 1–20, 2019.

25. G. A. Papagiannopoulos and G. D. Hatzigeorgiou, "On the use of the half-power bandwidth method to estimate damping in building structures," *Soil Dyn. Earthq. Eng.*, vol. 31, no. 7, pp. 1075–1079, 2011.

26. C. Leys, C. Ley, O. Klein, P. Bernard, and L. Licata, "Detecting outliers: Do not use standard deviation around the mean, use absolute deviation around the median," *J. Exp. Soc. Psychol.*, vol. 49, no. 4, pp. 764–766, 2013.

27. I. Antoniadis and G. Glossiotis, "Cyclostationary analysis of rolling-element bearing vibration signals," *J. Sound Vib.*, vol. 248, no. 5, pp. 829–

845, 2001.

28. J. Hebda-Sobkowicz, R. Zimroz, M. Pitera, and A. Wyłomańska, "Informative frequency band selection in the presence of non-Gaussian noise – a novel approach based on the conditional variance statistic with application to bearing fault diagnosis," *Mech. Syst. Signal Process.*, vol. 145, 2020.

29. A. Moshrefzadeh and A. Fasana, "The Autogram: An effective approach for selecting the optimal demodulation band in rolling element bearings diagnosis," *Mech. Syst. Signal Process.*, vol. 105, pp. 294–318, 2018.

30. Y. Wang, J. Xiang, R. Markert, and M. Liang, "Spectral kurtosis for fault detection, diagnosis and prognostics of rotating machines: A review with applications," *Mech. Syst. Signal Process.*, vol. 66–67, pp. 679–698, 2016.

31. X. Li, W. Zhang, and Q. Ding, "Understanding and improving deep learning-based rolling bearing fault diagnosis with attention mechanism," *Signal Processing*, vol. 161, pp. 136–154, 2019.

32. K. Simonyan and A. Zisserman, "Very deep convolutional networks for large-scale image recognition," *3rd Int. Conf. Learn. Represent. ICLR 2015 - Conf. Track Proc.*, pp. 1–14, 2015.

33. D. Pedamonti, "Comparison of non-linear activation functions for deep neural networks on MNIST classification task," *arXiv*, no. 3, 2018.

34. "No Title." [Online]. Available:

http://www.cwru.edu/laboratory/bearing/welcome_over view. html.

35. W. A. Smith and R. B. Randall, “Rolling element bearing diagnostics using the Case Western Reserve University data: A benchmark study,” *Mech. Syst. Signal Process.*, vol. 64–65, no. May 2015, pp. 100–131, 2015.

36. H. Kim and B. D. Youn, “A New Parameter Repurposing Method for Parameter Transfer with Small Dataset and Its Application in Fault Diagnosis of Rolling Element Bearings,” *IEEE Access*, vol. 7, pp. 46917–46930, 2019.

Abstract (Korean)

생성 신호를 활용한 해석 가능 인공지능 기반 베어링 고장 주파수 추정에 관한 연구

서울대학교 공과대학
기계항공공학부 대학원
최 종 현

베어링의 고장 신호가 특정 공진 주파수 대역에 진폭 변조 되기에 진폭 변조를 위한 주파수 대역을 선택하는 것은 포락 해석 기반의 베어링 고장 진단 분야에서 가장 중요한 부분이다. 최근까지, 많은 연구자들이 여러 도메인에서 공진 영역을 가르킬 수 있는 표지(indicator)들을 개발하였으며 이진 트리나 최적화 기법과 같은 방법으로 이 표지를 최대화 하는 방식으로 올바른 필터 영역을 추정하고자 하였다. 그러나, 이러한 표지들이 복잡한 신호처리 과정을 거쳐서 계산되기에 기존의 기법들은 필연적으로 표지 선택에 다량의 도메인 지식을 요하며 밴드 추출 과정에도 최적성과 실시간 진단 사이의 트레이드 오프(trade-off)가 발생하는 문제점이 있다. 이러한 문제를 해결하기 위하여 본 학위 논문에서는 생성 신호로 훈련된 1차원 어텐션 게이트 합성곱 신경망(1D-AttGCNN) 기반의 딥러닝 기법을 제안한다. 해당 모델은 생성 신호에서 사전에 정의된 공진 파라미터를 회귀하는 방법을 학습하며 진단 과정에서는 추가로 실제 데이터에 대한 훈련을 요하지 않는다. 또한 제안한 아키텍쳐는 어텐션 게이트를

포함하여, 자동으로 고장으로 발생하는 공진 영역을 국부화 시키는 방법을 학습할 수 있다. 또한 본 학위 논문에서는 신호 생성 과정에 불확실성과 비가우시안 노이즈를 고려하여 목표가 되는 실제 신호에 모델이 적응을 올바르게 하도록 하였다. 본 학위 논문에서는 제안 기법의 정합성은 세가지 케이스를 활용하여 여러 다른 공학적 환경에서 검증하였다. 또한, 기존의 빠른 컬토그램(Fast Kurtogram)과 오토그램(Autogram)이라는 기법과의 정량적인 비교 또한 포함되었다. 결과적으로 제안 기법은 기존에 기법에 비하여 우수한 진단 성능을 보여주었으며, 제안 아키텍처와 신호 생성 과정의 유효성 또한 검증 되었다.

주제어: 베어링 고장 진단(Bearing fault diagnosis)
포락 해석(Envelope analysis)
공진 주파수 선택(Resonance band selection)
집중 기법(Attention mechanism)
신호 생성(Signal generation)
합성곱 신경망(Convolutional neural network)

학 번: 2019-28698